One-sided composite cavity on an optical nanofiber for cavity QED

iD Ramachandrarao Yalla, iD K. Muhammed Shafi, Kali P. Nayak, et al.

View Online   Export Citation   CrossMark

ARTICLES YOU MAY BE INTERESTED IN

2.7 μm quantum cascade detector: Above band gap energy intersubband detection
Applied Physics Letters **120**, 071104 (2022); https://doi.org/10.1063/5.0076856

Demonstration of DC Kerr effect induced high nonlinear susceptibility in silicon rich amorphous silicon carbide
Applied Physics Letters **120**, 071107 (2022); https://doi.org/10.1063/5.0075852

Voltage control of magnetism with magneto-ionic approaches: Beyond voltage-driven oxygen ion migration
Applied Physics Letters **120**, 070501 (2022); https://doi.org/10.1063/5.0079762
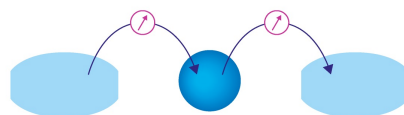
One-sided composite cavity on an optical nanofiber for cavity QED

View Online   Export Citation   CrossMark

Ramachandrarao Yalla,[1,a)] K. Muhammed Shafi,[2,b)] Kali P. Nayak,[2,c)] and Kohzo Hakuta[2]

AFFILIATIONS

[1]School of Physics, University of Hyderabad, Hyderabad, Telangana 500046, India
[2]Center for Photonic Innovations, University of Electro-Communications, Chofu, Tokyo 182-8585, Japan

[a)]Author to whom correspondence should be addressed: rrysp@uohyd.ac.in
[b)]Present address: Department of Instrumentation & Applied Physics, Indian Institute of Science, Bengaluru 560012, India.
[c)]Present address: Department of Engineering Science, University of Electro-Communications, Chofu, Tokyo 182-8585, Japan.

ABSTRACT

We demonstrate a one-sided cavity on an optical nanofiber (ONF) using a composite method. The one-sided composite cavity is created by mounting an asymmetric defect mode grating on an ONF. We design the one-sided composite cavity on an ONF to enhance channeling efficiency into one side of ONF while operating from under- to critical- and over-coupling regimes using numerical simulations. Experimentally, we demonstrate coupling characteristics of the one-sided composite cavity, showing good correspondence with simulation results.

Published under an exclusive license by AIP Publishing. https://doi.org/10.1063/5.0079624

The cavity quantum electrodynamics (QED) approach for enhancing light–matter interaction strength has attracted great interest with potential applications ranging from quantum optics,[1–4] quantum networks,[1,2] and sensing.[5] A crucial aspect of cavity QED is Purcell enhancement and unidirectional channeling of spontaneous emission of single quantum emitters to realize deterministic single photon sources.[6–10] Two types of cavity schemes have been discussed, such as two-sided and one-sided.[11] Formation of two/one-sided cavity schemes has been proposed and experimentally demonstrated in various geometries at micro-/nano-scales.[12–16] Examples include conventional Fabry–Pérot, diamond nanobeam,[6,7] microtoroid and bottle-neck,[17,18] silicon nitride photonic crystal (PhC),[7,19] and silica optical micro-/nano-fiber based cavities.[20–26] The formed cavities have been utilized for enhancing the spontaneous emission rate of single quantum emitters.[12–16]

Among the examples mentioned above, silica PhC optical nanofiber (ONF) cavities are particularly promising due to their ultra-low-loss coupling to conventional single-mode fibers for fiber-based quantum networks.[27,28] Regarding the formation of two-sided PhC cavities on silica ONFs, two methods have been proposed and experimentally demonstrated.[22–24,29–34] One is the direct fabrication of nanostructures on the surface of ONF itself using different techniques.[21–24] The other is a composite photonic crystal cavity (CPCC) method, wherein CPCC is created by combining a defect mode grating with an ONF.[3,29,30] CPCC method is particularly preferable for positioning the

solid-state quantum emitter to anti-node of cavity mode.[3] Precise tuning of cavity resonance wavelength up to ± 10 nm around the designed wavelength to match quantum emitter's spectral emission line has also been experimentally demonstrated.[23,35] PhC ONF cavities have been utilized for enhancing the spontaneous emission rate of single quantum emitters in the vicinity of an ONF.[3,4,23] These PhC ONF cavities are two-sided, and single photons are transmitted equally from both sides of the cavity on an ONF, i.e., both sides of ONF guided modes. The measured maximum channeling efficiency into either side of ONF guided mode was 32%–42%.[3,4]

A one-sided cavity will be crucial for practical applications based on single photon sources. The one-sided cavity can channel the total spontaneous emission of a single quantum emitter into one side of ONF guided modes. Moreover, various quantum information protocols are formulated based on one-sided cavity schemes.[13] Therefore, realizing one-sided cavities on ONFs is an essential requirement to extend for various quantum information applications. The one-sided PhC cavity on ONFs has not been experimentally demonstrated yet.

In this Letter, we report a systematic design and implementation of a one-sided composite cavity on an ONF. As conceptually displayed in Fig. 1(a), the essential point is to fabricate a nano-grating with a different number of slats on either side of the defect, defined as an asymmetric defect-mode grating (ADMG). Then, the one-sided composite cavity is formed by mounting ADMG on ONF. We numerically design
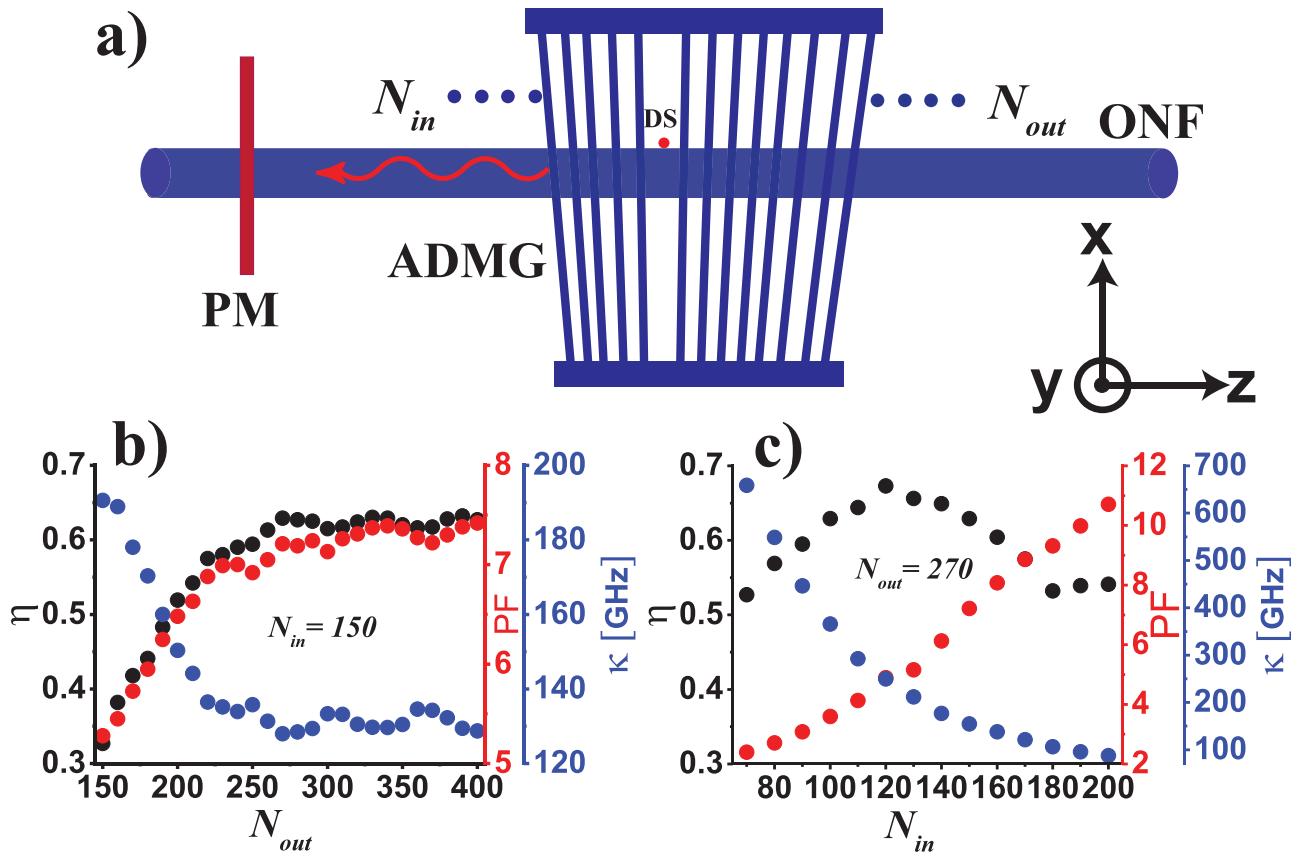
FIG. 1. (a) A conceptual top view of a one-sided composite cavity on an optical nanofiber (ONF). The one-sided composite cavity is formed by combining an ONF and an asymmetric defect mode grating (ADMG). N_{in}, N_{out}, PM, and DS denote input slat number, output slat number, power monitor, and dipole source, respectively. (b) and (c) show simulation predicted values for channeling efficiency (η, black dots), Purcell factor (PF, red dots), and total cavity linewidth (κ, blue dots) as a function of N_{out} and N_{in}-values, respectively. N_{in}-value is fixed at 150 for (b) and N_{out}-value is fixed at 270 for (c).

the composite cavity to enhance channeling efficiency into one side of ONF while operating from under- to critical- and over-coupling regimes with a minimum scattering loss by a varying number of slats at the input side of the cavity. Experimentally, we demonstrate coupling characteristics of the one-sided composite cavity, showing good correspondence with simulation results.

First, we discuss the design of a one-sided composite cavity. The conceptual diagram of a one-sided composite cavity on ONF is shown in Fig. 1(a). The cavity is formed by mounting ADMG onto ONF. The essential point is to design a nano-grating with different number of slats on either side of the defect. Additionally, we designed the ADMG with a diverged grating period for tuning the cavity resonance.[35] Simulations are performed using the finite difference time domain method.[35] We set a y-polarized dipole source (DS) on the surface of ONF at the anti-node position of the cavity, and a power monitor (PM) is placed sufficiently far from the DS position to measure the power (P_c) coupled into the guided mode. P and P_0 are the total power emitted by the DS in the presence of the cavity and the vacuum environment, respectively. We determine the Purcell factor (PF) and the channeling efficiency (η) as $PF = P/P_0$ and $\eta = P_c/P$, respectively. We find the optimum parameters by maximizing the η-value into the guided mode. We also simulate the cavity reflection spectra using a

mode source to infer the total cavity linewidth (κ) and the on-resonance reflection (R_0).

Design parameters for the one-sided composite cavity are ONF diameter ($2a$), grating period (Λ_g), defect-width ($w_g = 1.5\Lambda_g$), duty cycle (α), slat width ($t = \alpha\Lambda_g$), number of slats at the input side (N_{in}), and number of slats at the output side (N_{out}). We assume a rectangular slat shape with a slat depth of $2\,\mu$m and ADMG length to be $500\,\mu$m.[35] As per our previous work,[35] optimum parameters for the two-sided cavity were as follows: $2a = 510$ nm, $\Lambda_g = 252$ (± 5) nm, $w_g = 378.0$ (± 7.5) nm, $\alpha = 20\%$, $t = 50.4$ (± 1.0) nm, and total number of slats (N) = 300. The essential point was an equal number of slats on both sides of the defect, i.e., $N_{in} = N_{out} = 150$, where $N = N_{in} + N_{out}$ is total number of slats. The simulated η-value was same for both sides of ONF guided modes for two-sided cavity. The maximum η-value was 0.325 at one-side of ONF guided modes.

In the present design, we find optimum parameters for the one-sided composite cavity by simulating η-value, PF-value, and κ-value. A key point of the optimization is to choose optimum N_{in} and N_{out}-values while keeping scattering loss as small as possible to achieve η-value as maximum as possible at one side of ONF. By monitoring η and PF-values, N_{out}-value is swept from 150 to 400 with a step of 10 while keeping N_{in}-value fixed at 150. Summary of the simulated results

is plotted in Fig. 1(b). Black, red, and blue dots correspond to η, PF, and κ-values as a function of N_{out}-value, respectively. One can readily see that saturation behavior of η, PF, and κ-values for $N_{out} \geq 270$. η and PF-values are saturated for $\kappa \leq 130$ GHz.

By setting $N_{out} = 270$, N_{in}-value is swept from 70 to 200 with a step of 10. Summary of the simulated results is plotted in Fig. 1(c). Black, red, and blue dots correspond to η, PF, and κ-values as a function of N_{in}-value, respectively. One can readily see that κ-value decreases as N_{in}-value increases; consequently, PF-value increases as expected. However, the η-value peaks around $N_{in} = 120$ ($\kappa = 250$ GHz). Maximum η-value is found to be 0.673. Note that the present η-value is twice compared to the case for the two-sided cavity on the ONF.[35] The whole emission can be channeled into one side of ONF guided modes, useful for various single-photon applications. Thus, optimum input and output slat numbers for the one-sided composite cavity are $N_{in} = 120$ and $N_{out} \geq 270$, respectively. Note that the tunability of the presently designed cavity is ± 10 nm.

Regarding experimental realizations, optimized parameters for ADMG patterns are fabricated on a silica substrate using electron beam lithography and chemical etching.[3,29,30,35] By considering experimental imperfections, ADMG patterns are fabricated with $N_{out} = 390$ and N_{in}-value varied from 100 to 190 with a step size of 10. Note that patterns with different N_{in}-values are fabricated on the same silica substrate. The ONF is fabricated using heat and pull technique[27,30,37] and has a uniform waist region of 2.5 mm with a diameter of 510 ± 5 nm.[27,30,37] The measured optical transmission of the ONF is 98%.

A schematic of the experimental setup for optical characterization is shown in Fig. 2. We image the ADMG pattern through an objective lens (OL) by sending white light (WL) and observing using a charge-coupled device (CCD). ONF is positioned perpendicular to the slats using a rotational stage. The detailed procedure for the precise alignment of the ADMG pattern and its mounting onto ONF can be found in Refs. 3, 29, and 30. At the input side of the cavity, we launch a spectrally filtered supercontinuum (SC) light with a wavelength ranging from 600 to 700 nm through a polarizer (P) to ensure linear polarization. The polarized light is split into two beams with a ratio of 1:99 using a fiber beam splitter (FBS). One of the output sides (1% of the input signal) of the FBS is connected to the cavity through an in-line fiber polarizer (ILP) to control the light polarization angle. The resultant reflected signal is monitored through the other input side of

the same FBS with the transmission of 99% and recorded using a spectrum analyzer (SA) with a resolution of 0.05 nm (30 GHz).

Simulated and the corresponding measured one-sided composite cavity characteristics are shown in Figs. 3(a) and 3(b), respectively. Typical simulated cavity reflection spectra for $N_{in} = 100$, 180, and 220 are shown in Fig. 3(a)-1, 2, and 3, respectively. Blue (red) trace corresponds to x (y)-mode. One can readily see strong photonic reflection bands around 640 nm, along with dips at the center of the bands for all traces. We obtain cavity resonance wavelength (λ_0), cavity linewidth ($\Delta\lambda$), and on-resonance reflection (R_0) by fitting the dip in reflection spectra with Lorentzian. The x- and y-modes resonance dips are separated by 1.05 nm. We measured cavity reflection spectra at various N_{in}-values by un-mounting ADMG at one pattern and translating it to the other pattern for the next mounting. Typical measured cavity reflection spectra in Fig. 3(b)-1, 2, and 3 correspond to $N_{in} = 100$, 140, and 170, respectively. Note that due to experimental imperfections, N_{in} and N_{out}-values are different compared to simulation values. Blue (red) trace corresponds to x (y)-mode. We observed strong optical reflection bands around a wavelength of 627 nm in all traces, accompanied by dips at the center. Measured separation in λ_0-values for x- and y-modes is 1.30 nm. The total cavity linewidths ($\kappa = c\Delta\lambda/\lambda_0^2$, where c is velocity of light in free space) and quality factors ($Q = \lambda_0/\Delta\lambda$) are obtained from $\Delta\lambda$-values and λ_0-values. Simulated and the corresponding measured λ_0, $\Delta\lambda$, R_0, Q, and κ-values are summarized in Table I. Superscripts denote polarizations.

Regarding measured λ_0-values and separation for x- and y-modes, deviation from simulation values are mainly due to fabrication ambiguities in ONF diameter and ADMG parameters. As discussed in previous works,[3,35] using measured λ_0-value and fluctuations in the grating period, we estimate the ONF diameter to be 500 ± 4 nm,[35] implying that the ONF diameter is thinner than the value set in simulations. The changes required in ONF diameter indicate that the present results are within fabrication tolerances. However, it should be noted that the presently designed cavities can tune the λ_0-value up to ± 10 nm.[35] Although experimental discrepancies exist, measured reflection-band, clear polarization dependence, and cavity mode around the center of the reflection-band are in reasonable agreement with simulation predicted results. To have a quantitative evaluation of the designed cavity, we analyze coupling characteristics in the following.
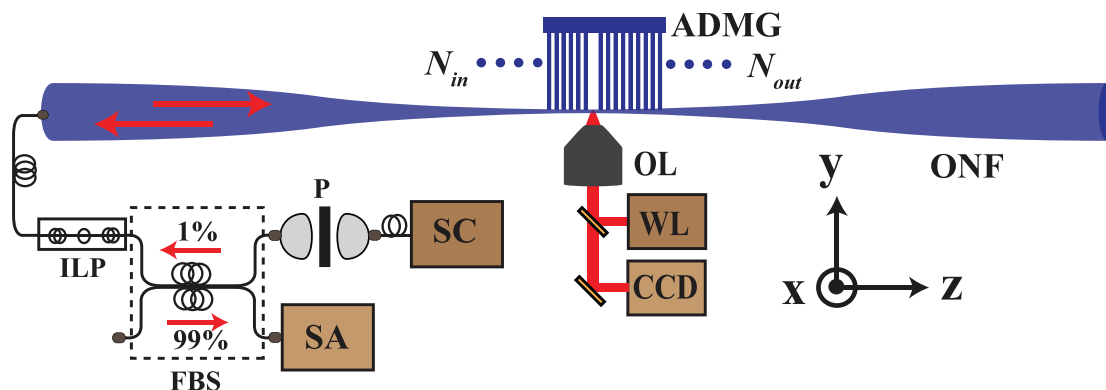

FIG. 2. A schematic of the experimental setup for measuring reflection spectra of a one-sided composite cavity. SC, P, ILP, FBS, OL, WL, CCD, and SA denote super-continuum source, polarizer, in-line polarizer, in-line fiber beam splitter, objective lens, white light source, charge-coupled device, and spectrum analyzer, respectively. N_{in} and N_{out} denote input slat number and output slat number of ADMG, respectively.
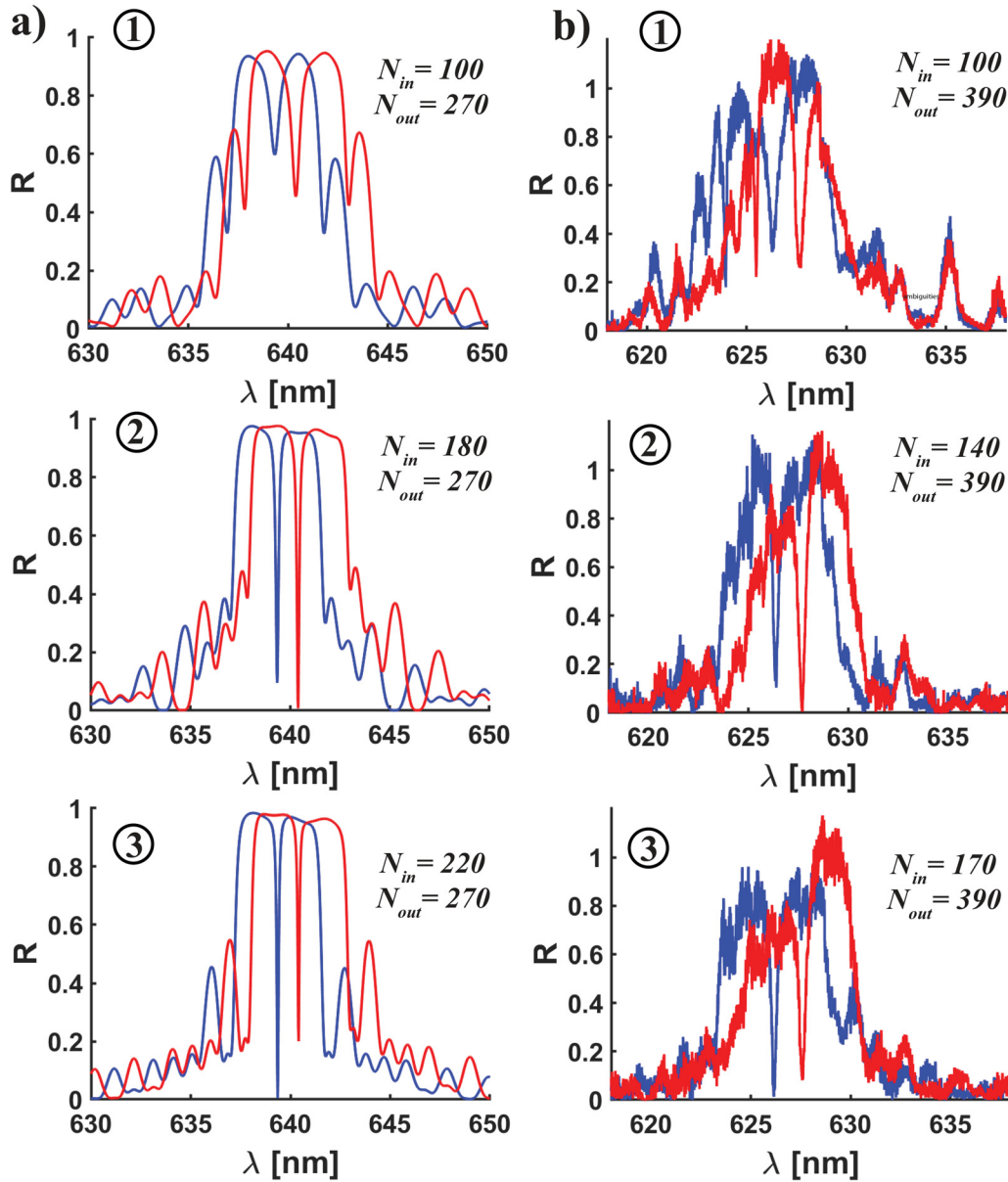
FIG. 3. Typical simulated and the corresponding measured results for a one-sided composite cavity on an optical nanofiber: (a) and (b) show simulated and measured cavity reflection spectra for x (blue trace) and y (red trace)-modes. 1, 2, and 3 correspond to different input slat number (N_{in}) at fixed output slat number (N_{out}) as mentioned in the figure.

Reflection amplitude (r) for one-sided cavity can be formulated[11,37] as

$$r = \frac{\frac{1}{2}(\kappa_{in} - \kappa_{sc}) - i\Delta\omega}{\frac{1}{2}(\kappa_{in} + \kappa_{sc}) + i\Delta\omega}, \qquad (1)$$

where κ_{in}, κ_{sc}, and $\Delta\omega = \omega - \omega_0$ are input coupling rate, scattering rate (intra-cavity loss rate), and detuning between the light source frequency (ω) and cavity resonance frequency (ω_0), respectively.

$\kappa = \kappa_{in} + \kappa_{sc}$ is the total cavity linewidth. The reflectivity is $R = |r|^2$. On-resonance ($\Delta\omega = 0$) reflectivity (R_0) can be written as

$$R_0 = \left|\frac{\kappa_{in} - \kappa_{sc}}{\kappa}\right|^2 = \left|1 - \frac{2\kappa_{sc}}{\kappa}\right|^2. \qquad (2)$$

The above equation implies that as κ-value decreases, R_0-value decreases in the over-coupling regime ($\kappa/2 > \kappa_{sc}$), reaches zero at critical-coupling ($\kappa/2 = \kappa_{sc} = \kappa_{in}$), and increases in the under-coupling regime ($\kappa/2 < \kappa_{sc}$).

TABLE I. Summary of typical simulated and measured parameters for the one-sided composite cavity on an optical nanofiber.

	N_{in}	λ_0 [nm]		$\Delta\lambda$ [nm]		R_0		Q		κ [GHz]	
		λ_0^x	λ_0^y	$\Delta\lambda^x$	$\Delta\lambda^y$	R_0^x	R_0^y	Q^x	Q^y	κ^x	κ^y
Simulation	100	639.33	640.38	0.552	0.500	0.595	0.453	1158	1280	405	365
	180	639.33	640.38	0.167	0.146	0.095	0.008	3828	4386	122	107
	220	639.33	640.38	0.109	0.100	0.004	0.200	5870	6404	79	73
Experiment	100	626.30 ± 0.05	627.60 ± 0.05	0.83 ± 0.08	0.61 ± 0.06	0.33 ± 0.04	0.26 ± 0.03	754 ± 50	1028 ± 90	635 ± 60	464 ± 50
	140	626.38 ± 0.05	627.66 ± 0.05	0.47 ± 0.04	0.39 ± 0.03	0.15 ± 0.06	0.02 ± 0.001	1332 ± 90	1610 ± 120	358 ± 30	297 ± 35
	170	626.20 ± 0.05	627.55 ± 0.05	0.30 ± 0.04	0.32 ± 0.05	0.02 ± 0.01	0.08 ± 0.01	2087 ± 140	1960 ± 130	230 ± 50	244 ± 30

Simulated and the corresponding measured coupling characteristics of the present cavity are summarized in Figs. 4(a) and 4(b), respectively. Simulated R_0-values as a function of κ-values are plotted in Fig. 4(a). Blue (red) dots correspond to x (y)-mode. N_{in}-value is varied from 70 to 240 (70 to 220) for x (y)-mode. To infer scattering limited decay rate (κ_{sc}) of the formed cavity, we fit simulation predicted R_0-values with κ_{sc}-value as free parameter using Eq. (2). Fitted result for x (y)-mode R_0-values is shown by the blue (red) solid line. For x (y)-mode, obtained κ_{sc}-value is 43 GHz (54 GHz). Obtained κ_{sc}-value for y-mode is higher than that for x-mode due to a higher scattering loss of y-mode.

We measured cavity reflection spectra for N_{in}-value from 100 to 190, i.e., various κ-values. Measured R_0-values behavior is shown in Fig. 4(b). Blue (red) dots correspond to x (y)-mode. The origin of horizontal error bars is mainly due to the mounting uncertainty of ADMG onto ONF during experiments and the resolution of the spectrum analyzer used for measurements. The origin of vertical error bars is mainly due to power fluctuations of injected supercontinuum light source used for measurements. By increasing N_{in}-value, i.e., decreasing κ-value, we clearly observe R_0-value transition from over- to- critical- and under-coupling regimes as predicted by simulations. One can readily see the expected behavior of R_0-values for x (y)-mode as predicted by simulations. We estimate κ_{sc}-value by fitting Eq. (2) to the measured R_0-values. Blue (red) solid line is the fitted result for x (y)-mode R_0-values. For x (y)-mode, obtained κ_{sc}-value is 107 ± 8 (136 ± 10 GHz). Note that measured κ_{sc}-value for y-mode is higher than that for x-mode as predicted by simulations.

Regarding measured κ_{sc}-value, deviation from the simulation predicted value is mainly due to the fabrication ambiguities in ONF diameters and ADMG parameters, leading to a higher scattering loss. Using κ_{sc}-value and effective cavity length (l) of 22 μm, we estimate scattering limited cavity quality factor ($Q_{sc} = \frac{c}{\lambda_0 \kappa_{sc}}$), cavity finesse ($\mathscr{F}_{sc} = \frac{c}{2l\kappa_{sc}}$), and one-pass power loss ($\mathscr{L} = 1 - e^{-2\pi\kappa_{sc}l/c}$). Simulated and measured Q_{sc}, $\mathscr{F}_{sc}$, and $\mathscr{L}$-values are summarized in Table II. Superscripts denote polarizations. Note that the simulated Q_{sc} and $\mathscr{F}_{sc}$ ($\mathscr{L}$)-values give an upper (lower) bound on cavity performance for both polarizations. Measured $\mathscr{L}$-value mainly indicates insertion loss due to ADMG as the ONF loss is much lower than 2%. Simulated and measured results clearly demonstrate that ADMG does not introduce significant losses while forming a one-sided composite cavity on ONF. Q_{sc}, $\mathscr{F}_{sc}$, and $\mathscr{L}$-values can be improved by designing ADMG to
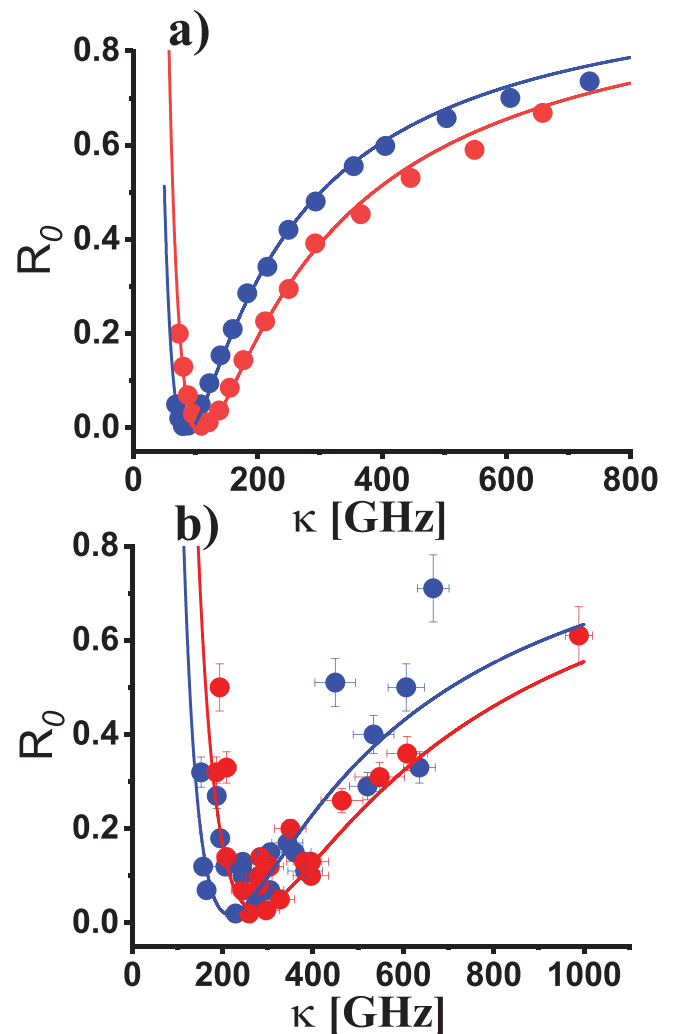

FIG. 4. Simulated and the corresponding measured results for on-resonance reflection (R_0)-values. (a) and (b) show simulated and measured R_0-values as a function of total cavity linewidth (κ). Blue (red) dots correspond to x (y)-mode. Blue (red) solid lines are fit to the data.

TABLE II. Simulated and measured performance parameters for the one-sided composite cavity on optical nanofiber.

	κ_{sc} [GHz]		Q_{sc}		$\mathscr{F}_{sc}$		$\mathscr{L}$ [%]	
	κ_{sc}^x	κ_{sc}^y	Q_{sc}^x	Q_{sc}^y	$\mathscr{F}_{sc}^x$	$\mathscr{F}_{sc}^y$	$\mathscr{L}^x$	$\mathscr{L}^y$
Simulation	43	54	10 900	8680	155	124	2.0	2.5
Experiment	107 ± 8	136 ± 10	4478 ± 334	3518 ± 260	62 ± 4	49 ± 3	4.9 ± 0.4	6.2 ± 0.5

produce an apodization index modulation.[22,38] It should be noted that high channeling efficiency can still be realized in the over-coupling regime with κ-value in the range 400–600 GHz [see Fig. 1(c)]. Therefore, the present cavity can be implemented for efficient unidirectional single photon generation using solid-state single quantum emitters. Note that unidirectional channeling of single photons can also be achieved based on chiral interactions,[39] but it can only control the photon flux into one side. In contrast, the one-sided cavity method is to enhance the unidirectional channeling efficiency and Purcell enhancement to realize deterministic single-photon sources.[6–10]

In summary, we have demonstrated a one-sided composite cavity on an ONF. Numerical and experimental results have clearly shown that the composite method can be extended to a one-sided cavity scheme without any significant scattering losses. The presently designed one-sided composite cavity can channel total spontaneous emission into one side of ONF. Thus, the designed one-sided composite cavity with a narrow bandwidth single quantum emitter may open new routes in nanofiber quantum photonics.[36,40–42] The one-sided cavity can be advantageous for practical device design and applications in quantum information science.

AUTHOR DECLARATIONS
Conflict of Interest
The authors declare that they have no conflict of interest.

DATA AVAILABILITY
The data that support the findings of this study are available from the corresponding author upon reasonable request.

REFERENCES

[1]S. Ritter, C. Nölleke, C. Hahn, A. Reiserer, A. Neuzner, M. Uphoff, M. Mücke, E. Figueroa, J. Bochmann, and G. Rempe, Nature **484**, 195 (2012).
[2]H. J. Kimble, Nature **453**, 1023 (2008).
[3]R. R. Yalla, M. Sadgrove, K. P. Nayak, and K. Hakuta, Phys. Rev. Lett. **113**, 143601 (2014).
[4]K. P. Nayak, J. Wang, and J. Keloth, Phys. Rev. Lett. **123**, 213602 (2019).
[5]D. Yang, B. Duan, X. Liu, A. Wang, X. Li, and Y. Ji, Micromachines **11**, 72 (2020).
[6]T. G. Tiecke, J. D. Thompson, N. P. de Leon, L. R. Liu, V. Vuletić, and M. D. Lukin, Nature **508**, 241 (2014).
[7]J. D. Thompson, T. G. Tiecke, N. P. de Leon, J. Feist, A. V. Akimov, M. Gullans, A. S. Zibrov, V. Vuletic, and M. D. Lukin, Science **340**, 1202 (2013).
[8]J. M. Raimond, M. Brune, and S. Haroche, Rev. Mod. Phys. **73**, 565 (2001).
[9]D. Englund, A. Faraon, I. Fushman, N. Stoltz, P. Petroff, and J. Vučković, Nature **450**, 857–861 (2007).
[10]I. Fushman, D. Englund, A. Faraon, N. Stoltz, P. Petroff, and J. Vučković, Science **320**, 769 (2008).
[11]D. F. Walls and G. J. Milburn, *Quantum Optics* (Springer, Berlin, 2008).
[12]K. Vahala, Nature **424**, 839–846 (2003).
[13]A. Reiserer and G. Rempe, Rev. Mod. Phys. **87**, 1379 (2015).
[14]C. Liu, Y. Sun, L. Zhao, S. Zhang, M. M. T. Loy, and S. Du, Phys. Rev. Lett. **113**, 133601 (2014).
[15]S. Kato and T. Aoki, Phys. Rev. Lett. **115**, 093603 (2015).
[16]J. Gallego, W. Alt, T. Macha, M. Martinez-Dorantes, D. Pandey, and D. Meschede, Phys. Rev. Lett. **121**, 173603 (2018).
[17]T. Aoki, B. Dayan, E. Wilcut, W. P. Bowen, A. S. Parkins, T. J. Kippenberg, K. J. Vahala, and H. J. Kimble, Nature **443**, 671–674 (2006).
[18]C. Junge, D. O'Shea, J. Volz, and A. Rauschenbeutel, Phys. Rev. Lett. **110**, 213604 (2013).
[19]S.-P. Yu, J. D. Hood, J. A. Muniz, M. J. Martin, R. Norte, C.-L. Hung, S. M. Meenehan, J. D. Cohen, O. Painter, and H. J. Kimble, Appl. Phys. Lett. **104**, 111103 (2014).
[20]M. Sumetskya, Y. Dulashko, J. M. Fini, and A. Hale, Appl. Phys. Lett. **86**, 161108 (2005).
[21]K. P. Nayak, F. L. Kien, Y. Kawai, K. Hakuta, K. Nakajima, H. T. Miyazaki, and Y. Sugimoto, Opt. Express **19**, 14040–14050 (2011).
[22]K. P. Nayak and K. Hakuta, Opt. Express **21**, 2480 (2013).
[23]A. W. Schell, H. Takashima, S. Kamioka, Y. Oe, M. Fujiwara, O. Benson, and S. Takeuchi, Sci. Rep. **5**, 9619 (2015).
[24]W. Li, J. Du, V. G. Truong, and S. Nic Chormaic, Appl. Phys. Lett. **110**, 253102 (2017).
[25]P. Schneeweiss, S. Zeiger, T. Hoinkes, A. Rauschenbeutel, and J. Volz, Opt. Lett. **42**, 85–88 (2017).
[26]P. Qing, J. Gong, X. Lin, N. Yao, W. Shen, A. Rahimi-Iman, W. Fang, and L. Tong, Appl. Phys. Lett. **114**, 021106 (2019).
[27]K. P. Nayak, M. Sadgrove, R. R. Yalla, F. L. Kien, and K. Hakuta, J. Opt. **20**, 073001 (2018).
[28]R. R. Yalla, F. L. Kien, M. Morinaga, and K. Hakuta, Phys. Rev. Lett. **109**, 063602 (2012).
[29]M. Sadgrove, R. R. Yalla, K. P. Nayak, and K. Hakuta, Opt. Lett. **14**, 2542 (2013).
[30]J. Keloth, M. Sadgrove, R. R. Yalla, and K. Hakuta, Opt. Lett. **40**, 4122 (2015).
[31]H. Takashima, M. Fujiwara, A. W. Schell, and S. Takeuchi, Opt. Express **24**, 15050–15058 (2016).
[32]W. Li, J. Du, and S. N. Chormaic, Opt. Lett. **43**, 1674–1677 (2018).
[33]T. Tashima, H. Takashima, and S. Takeuchi, Opt. Express **27**, 27009–27016 (2019).
[34]P. Romagnoli, M. Maeda, J. M. Ward, V. G. Truong, and S. N. Chormaic, Appl. Phys. B **126**, 111 (2020).
[35]R. R. Yalla and K. Hakuta, Appl. Phys. B **126**, 187 (2020).
[36]K. M. Shafi, W. Luo, R. R. Yalla, K. Iida, E. Tsutsumi, A. Miyanaga, and K. Hakuta, Sci. Rep. **8**, 13494 (2018).
[37]J. Keloth, K. P. Nayak, and K. Hakuta, Opt. Lett. **42**, 1003 (2017).
[38]Q. Quan, P. B. Deotare, and M. Loncar, Appl. Phys. Lett. **96**, 203102 (2010).
[39]P. Lodahl, S. Mahmoodian, S. Stobbe, A. Rauschenbeutel, P. Schneeweiss, J. Volz, H. Pichler, and P. Zoller, Nature **541**, 473–480 (2017).
[40]M. Sadgrove and K. P. Nayak, New J. Phys. **19**, 063003 (2017).
[41]K. M. Shafi, K. P. Nayak, A. Miyanaga, and K. Hakuta, Appl. Phys. B **126**, 58 (2020).
[42]E. Neu, D. Steinmetz, J. Riedrich-Moller, S. Gsell, M. Fischer, M. Schreck, and C. Becher, New J. Phys. **13**, 025012 (2011).